

GridPE: Unifying Positional Encoding in Transformers with a Grid Cell-Inspired Framework

Boyang Li^{*1}, Yulin Wu^{*1}, Nuoxian Huang¹, Wenjia Zhang²

¹Behavioral and Spatial AI Lab, Peking University, ²College of Architecture and Urban Planning, Tongji University,
liboyang@stu.pku.edu.cn, cover.wu@stu.pku.edu.cn, huangnx0927@stu.pku.edu.cn,
wenjiazhang@tongji.edu.cn

Abstract

Understanding spatial location and relationships is a fundamental capability for modern artificial intelligence systems. Insights from human spatial cognition provide valuable guidance in this domain. Neuroscientific discoveries have highlighted the role of grid cells as a fundamental neural component for spatial representation, including distance computation, path integration, and scale discernment. In this paper, we introduce a novel positional encoding scheme inspired by Fourier analysis and the latest findings in computational neuroscience regarding grid cells. Assuming that grid cells encode spatial position through a summation of Fourier basis functions, we demonstrate the translational invariance of the grid representation during inner product calculations. Additionally, we derive an optimal grid scale ratio for multi-dimensional Euclidean spaces based on principles of biological efficiency. Utilizing these computational principles, we have developed a Grid-cell inspired Positional Encoding technique, termed *GridPE*, for encoding locations within high-dimensional spaces. We integrated GridPE into the Pyramid Vision Transformer architecture. Our theoretical analysis shows that GridPE provides a unifying framework for positional encoding in arbitrary high-dimensional spaces. Experimental results demonstrate that GridPE significantly enhances the performance of transformers, underscoring the importance of incorporating neuroscientific insights into the design of artificial intelligence systems. Our code can be accessed via the following anonymous link: <https://anonymous.4open.science/r/gridpe-vision-DCF0/>

Introduction

Understanding how the mammalian brain represents spatial characteristics and relationships remains a critical question in cognitive science and neuroscience. Specifically, the focus is on identifying the neural bases and their roles in self-localization, navigation, and path planning. Scholars have conducted extensive research to address this question. (Tolman 1948) designed an animal experiment where rats performed a wayfinding task in a radial maze, introducing the concept of the *cognitive map* to describe the internal environmental representation that supports flexible spatial behavior. Subsequent discoveries identified the neural cellular

basis of the cognitive map in the mammalian brain, a line of research that earned the Nobel Prize in 2014. Place cells activate when a mammal enters an area near a specific spatial location (O’keefe and Nadel 1978; Solstad, Moser, and Einevoll 2006), and are believed to distinguish and represent different places. Grid cells in the medial entorhinal cortex (MEC), on the other hand, exhibit periodic, hexagonal, and grid-like firing fields (Hafting et al. 2005). These cells are thought to define distance metrics in Euclidean space, support multi-scale self-localization, and facilitate path integration and vector-based navigation (Gorchetnikov and Grossberg 2007; Moser, Kropff, and Moser 2008; Banino et al. 2018). In other words, grid cells represent spatial relationships independently of the agent’s current visual sensory input and head direction (referred to as “allocentric” representation). Due to their close association with spatial representation, the principles of grid cell firing have been widely adopted by artificial intelligence researchers beyond neuroscience, including in robotics navigation system design (Yuan et al. 2015), reinforcement learning agent trajectory planning (Yu, Behrens, and Burgess 2020), and positional encoding for geospatial data (Mai et al. 2020, 2023).

There are at least two approaches to incorporating grid cells into AI systems. For bottom-up approach, agents can learn from trajectory experience (i.e., model training in the context of machine learning), and grid-like firing patterns can often emerge from certain neuron activations in the architecture (Banino et al. 2018; Whittington et al. 2022). While these agent architectures validate the existence of grid cells, they struggle to directly encode spatial positions from knowledge of the model. For the top-down methods, researchers intentionally design computational models to simulate grid cell firing and integrate them into the agent for navigation. Two commonly adopted techniques are the continuous attractor network (CAN) and the velocity-controlled oscillator (VCO). The CAN model constructs a recurrent neural network that takes velocity input to compute a steady state from this neural dynamic system, simulating grid cells (Burak and Fiete 2009). However, CAN presumes symmetric connections and regular cellular arrangement in the network, which rarely hold true in authentic neural anatomical structure (Anselmi, Murray, and Franceschiello 2020). VCO models assume that grid cell firing patterns arise from the interference of oscillations with distinct frequencies (Burgess,

^{*}These authors contributed equally.

Barry, and O’keefe 2007). A grid cell’s activation pattern can be the summation of three planar waves with respective frequency direction vectors, each separated by 120° (Blair, Welday, and Zhang 2007). VCO models encode location with high simplicity and are theoretically supported by neuroscience evidence such as band cells (Krupic, Burgess, and O’Keefe 2012) and phase precession phenomena in bats (Eliav et al. 2018; Yartsev, Witter, and Ulanovsky 2011).

Building on the advantages of the VCO model for explaining grid cells, this paper mathematically models grid cells based on VCO model assumptions. The activation intensity of a grid cell within a high-dimensional Euclidean space can be derived as the summation of Fourier basis functions. For example, a one-dimensional Euclidean space can be represented by one Fourier basis, while a two-dimensional Euclidean space can be represented by three Fourier bases. We first prove that the inner product of two grid cells can map to the metric endowed on Euclidean space, and we further demonstrate that grid cells can be represented as multi-dimensional vectors through Random Fourier Feature (RFF) computation. Following the economic principle of achieving the highest spatial resolution with the fewest cells, we derived the theoretically optimal scale ratio.

Inspired by the spatial encoding properties of grid cells, we designed a positional encoding scheme named GridPE for representing multi-dimensional spatial positions in self-attention architectures. To compare GridPE with classical positional encoding techniques, we conducted experiments using classic architectures such as Vision Transformer (ViT) and Pyramid Vision Transformer (PVT) architecture (Wang et al. 2021) on the ImageNet-100 image classification task (Deng et al. 2009). The results demonstrate its effectiveness in enhancing the self-attention mechanism by providing both absolute and relative positional information, highlighting the potential of integrating neuroscience findings into AI system design.

Preliminaries

We model the grid cell on the theoretical basis of VCO theory (Burgess, Barry, and O’keefe 2007; Hasselmo 2008). Under this assumption, presynaptic cells of the grid cell (sometimes referred to as “simple cells” (Anselmi, Murray, and Franceschiello 2020)) perform oscillations similar to two-dimensional planar waves, forming parallel band “strips” along specific directions. The oscillation frequency of the presynaptic dendrites is sensitive to the agent’s current velocity, which is why the theory is named “velocity-controlled.” The frequency can be expressed as the result of modulating the somatic oscillation base frequency, with the modulation magnitude depending on the velocity vector and the presynaptic preferred direction (or wave vector of the planar wave) (Yu, Behrens, and Burgess 2020).

$$\frac{d}{dt}\varphi = \omega_d = \omega_s + \beta \mathbf{v}^T \mathbf{k} \quad (1)$$

where ω_s is the somatic base frequency, usually experimentally measured as theta wave frequency (4-11 Hz) (Yu,

Behrens, and Burgess 2020). $\mathbf{v}, \mathbf{k} \in \mathbb{R}^2$ are the velocity vector and wave vector in the two-dimensional space, the latter indicating preferred direction and wave length. β is a position factor deciding sensitivity to velocity. The velocity-modulated dendrite frequency ω_d is the derivative of oscillation phase ϕ . Here, we do not differentiate between angular velocity and frequency due to their constant ratio of 2π . When we integrate the modulated frequency over the time t , we obtain the oscillation phase:

$$\varphi(t) - \varphi(0) = \int_0^t (\omega_s + \beta \mathbf{v}^T \mathbf{k}) dt = \omega_s t + \beta \mathbf{k}^T \mathbf{x} \quad (2)$$

Where \mathbf{x} is the displacement vector from time 0 to time t . Clearly, at a given time, locations with the same projection onto the wave vector correspond to the same oscillation phase, thus forming parallel activation bands across the environment when we calculate the amplitude. If we overlap multiple such presynaptic firing fields with weights, we can obtain grid cell hexagonal firing patterns. The oscillation is expressed as a Fourier basis function, and grid cell activation at any location can be expressed as (Dang et al. 2021):

$$\begin{aligned} g &= \sum_{i=1}^n c_i \cos(\varphi_i(t)) \\ &= \sum_{i=1}^n \frac{c_i}{2} \left(e^{j\varphi_i(t)} + e^{-j\varphi_i(t)} \right) \end{aligned} \quad (3)$$

Here, for the Fourier basis transformation, we consider only the positive frequency components and ignore the negative frequency components. In the context of grid cells, the positive frequency components are sufficient to describe the spatial periodicity and the phase relationships that give rise to the hexagonal grid pattern. The negative frequency components do not provide additional unique information about the grid cell firing patterns. By focusing on the positive frequency components, we simplify the mathematical representation without losing any essential information about the grid cell activation.

$$\begin{aligned} g &= \sum_{i=1}^n \frac{c_i}{2} e^{j\varphi_i(t)} \\ &= \sum_{i=1}^n \frac{c_i}{2} e^{j(\omega_s t + \beta \mathbf{k}_i^T \mathbf{x})} \\ &= \sum_{i=1}^n \frac{c_i}{2} e^{j\omega_s t} \cdot e^{j\beta \mathbf{k}_i^T \mathbf{x}} \\ &= \sum_{i=1}^n \tilde{c}_i(t) e^{j\mathbf{k}_i^T \mathbf{x}} \end{aligned} \quad (4)$$

The imagery unit is denoted as j , and the number of presynaptic cells is denoted as n . We omit the parameter β , which can be integrated into the wave vector \mathbf{k} . The time-dependent function $\tilde{c}_i(t)$ combines the information of synaptic weight and somatic base oscillation, while the factor of the Fourier basis depends only on the location \mathbf{x} . This implies that the

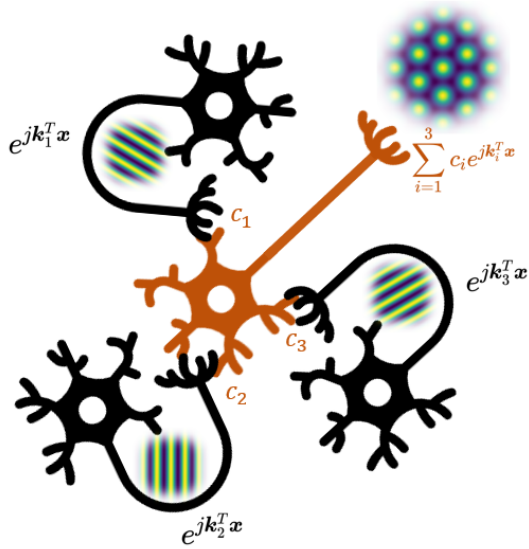


Figure 1: Illustration of VCO theory. The black neurons are presynaptic neurons with simple oscillation in their dendrites. The orange neuron is the grid cell, whose grid firing pattern results from the summation of the three oscillation with different preferred direction.

temporal fluctuation of the activation is driven solely by the intrinsic theta waves evolving over time, which are independent of spatial representation. Consequently, we can fix a certain time point and analyze the grid cell representation across space from a static viewpoint, omitting the time variable t in the subsequent derivation.

Previous research commonly utilizes three Fourier bases with directional preferences forming 120° angles between each other (Dang et al. 2021; Blair, Welday, and Zhang 2007), as illustrated in Figure 1. This arrangement of grid cells forming 120° angles results in a hexagonal lattice structure. Such a hexagonal arrangement is advantageous because it allows for the most efficient and uniform coverage of two-dimensional space, minimizing overlap and maximizing the distinctness of each cell’s spatial representation. This geometric efficiency is crucial for robust spatial navigation and representation, providing a highly regular and repeating pattern that facilitates the precise encoding of an animal’s environment and location.

Derivation of Grid Cell Positional Encoding

Inner Product Translational Invariance

Grid cells are not only responsible for representing absolute locations in Euclidean space but are also expected to encode relative spatial shifts between locations. This allows for the representation of free vectors from any starting location within the space, thereby facilitating vector-based navigation. The inner product of grid cell representations provides valuable insights into this capability. For a single grid cell, its representation at location \mathbf{x} is given by:

$$g(\mathbf{x}) = \sum_{i=0}^n c_i e^{j\mathbf{k}_i^T \mathbf{x}} \quad (5)$$

Assume that \mathbf{x} deviates from \mathbf{y} by a fixed vector \mathbf{d} (i.e., $\mathbf{x} - \mathbf{y} = \mathbf{d}$). We then compute the functional inner product of $g(\mathbf{x})$ with itself over the Euclidean space, that is.

$$\begin{aligned} \langle g(\mathbf{x}), g(\mathbf{y}) \rangle_{\mathcal{H}} &= \int_{\mathcal{X}} \sum_{i=0}^n \sum_{m=0}^n c_i c_m^* e^{j(\mathbf{k}_i - \mathbf{k}_m)^T \mathbf{x}} e^{j\mathbf{k}_m^T (\mathbf{x} - \mathbf{y})} \\ &= \sum_{i=0}^n |c_i|^2 e^{j\mathbf{k}_i^T \mathbf{d}} \end{aligned} \quad (6)$$

That means for a given grid cell, the inner product of its activation map and its shifted version can represent the shift vector without consideration of any certain locations. Apparently, the inner product form a translational invariant kernel function $\kappa_0(\mathbf{x}, \mathbf{y}) = \langle g(\mathbf{x}), g(\mathbf{y}) \rangle_{\mathcal{H}} = h(\mathbf{x} - \mathbf{y})$. There are countless grid cells in the mammal’s brain. The collective representation to the offset vector \mathbf{d} can be expressed as follow as the summation of grid cell inner products:

$$\begin{aligned} \sum_{g \in \mathcal{G}} \langle g(\mathbf{x}), g(\mathbf{y}) \rangle_{\mathcal{H}} &= \sum_i |c_i|^2 e^{j\mathbf{k}_i^T \mathbf{d}} \\ &\propto \int_{\mathbb{R}^2} p(\mathbf{k}) |c(\mathbf{k})|^2 e^{j\mathbf{k}^T \mathbf{d}} d\mathbf{k} \end{aligned} \quad (7)$$

Note this function is also a translational invariant kernel for \mathbf{x} and \mathbf{y} . Simultaneously, in its form it scale to the inverse Fourier transformation of the probability distribution of wave vectors. According to *Bochner theorem* (Bochner 2005), we know this kernel, as the inverse Fourier transformation of a non-negative measurement, is positive definite. Therefore, we can apply random Fourier feature (RFF) (Rahimi and Recht 2007) technique on this shift-invariant kernel, which demands positive definite kernel as the prerequisite. We denote the $\kappa(\mathbf{x}, \mathbf{y})$ as this kernel and we can know:

$$\begin{aligned}
\kappa(\mathbf{x}, \mathbf{y}) &= \int_{\mathbb{R}^2} p(\mathbf{k}) |c(\mathbf{k})|^2 e^{j\mathbf{k}^T \mathbf{d}} d\mathbf{k} \\
&= \mathbb{E}_{\mathbf{k}} \left[|c(\mathbf{k})|^2 e^{j\mathbf{k}^T \mathbf{d}} \right] \\
&\approx \frac{1}{D} \sum_{i=1}^D \left(|c_i|^2 e^{j\mathbf{k}_i^T \mathbf{x}} \cdot e^{-j\mathbf{k}_i^T \mathbf{y}} \right) \\
&= \frac{1}{\sqrt{D}} \begin{pmatrix} e^{j\mathbf{k}_1^T \mathbf{x}} \\ e^{j\mathbf{k}_2^T \mathbf{x}} \\ \vdots \\ e^{j\mathbf{k}_D^T \mathbf{x}} \end{pmatrix}^T \\
&\quad \cdot \begin{bmatrix} |c_1|^2 & & & \\ & |c_2|^2 & & \\ & & \ddots & \\ & & & |c_D|^2 \end{bmatrix} \\
&\quad \cdot \begin{pmatrix} e^{-j\mathbf{k}_1^T \mathbf{y}} \\ e^{-j\mathbf{k}_2^T \mathbf{y}} \\ \vdots \\ e^{-j\mathbf{k}_D^T \mathbf{y}} \end{pmatrix} \frac{1}{\sqrt{D}}
\end{aligned} \tag{8}$$

When considering the population activity of grid cells, we can disregard the constant $\frac{1}{\sqrt{D}}$ that represents the population size. In this context, grid cells can be seen as the product of diagonalized input weights and a vector whose entries are Fourier bases with preferred directional preferences. This is analogous to Fourier analysis, where a function is decomposed into orthogonal bases and their corresponding coefficients. Consequently, the inner product of spatial-domain representation functions in the functional space is replaced by the inner product of frequency-domain vectors in a finite-dimensional vector space.

We propose that the brain represents Euclidean space using multi-dimensional Fourier analysis, akin to the auditory system's processing of sound waves and the visual system's processing of light waves. By integrating oscillations of various spatial frequencies, the grid cell encoding system can efficiently represent spatial information with high resolution. Furthermore, the Random Fourier Features (RFF) approach imposes no constraints on the dimensionality of locations \mathbf{x} and \mathbf{y} . This suggests that the Fourier representation of grid cells can encode location information in arbitrarily high-dimensional spaces.

Optimal Ratio of Grid Scale under Economy Principle

In the derivation above, we assumed the wave vector (i.e., the preferred direction) follows a probability distribution, such as the uniform distribution often used in RFF. However, neuroscience evidence shows that the medial entorhinal cortex consists of several modules. Within the same module, the direction and period scale of the cell grids remain consistent, but these discretized scales shrink along the ventral-dorsal axis (Stensola et al. 2012), representing a transition

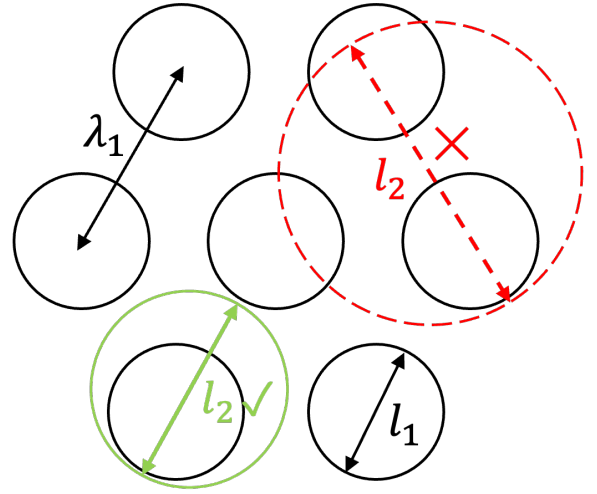


Figure 2: Illustration of relationship between firing fields diameter and periodicity. For two grid cells with adjacent discrete scale, the periodicity of the smaller scale must be less than the diameter of the larger one, otherwise the system cannot distinguish two locations.

from coarse, low-frequency to granular, high-frequency spatial information. The periodic ratio of the adjacent scale remains around 1.5, as estimated by both animal measurements and computational simulations (Stensola et al. 2012; Banino et al. 2018). This hierarchical spatial representation demands significantly fewer grid cells while maintaining fine spatial resolution, or say the economy principle (Wei, Prentice, and Balasubramanian 2015).

The challenge now is to determine the optimal ratio of the grid scale, which is crucial for constructing a positional encoding system. Recall that in the original positional encoding of the Transformer architecture (Vaswani et al. 2017), the encoding spatial frequency is calculated as $\omega_k = \frac{1}{10000^{2k/d}}$, forming a geometric series of wavelengths. The rationale behind this choice remains unclear, and we anticipate that computational theories of grid cells can provide insights into frequency determination.

Here we provide a generalized derivation based on the proof in (Wei, Prentice, and Balasubramanian 2015). We aim to represent p -dimensional Euclidean space with the least number of grid cells, reflecting the principle of economy. Assume there are m scales (or layers) of the grid cells. The period of the i -th module layer ($i = 1, 2, \dots, m$), or the distance between the adjacent grid vertices, is denoted as λ_i . The period increase as i becomes larger. The scale ratio of the adjacent layers is $r = \lambda_{i+1}/\lambda_i > 1$. A grid field is a hyperspherical area centered around a grid vertex in the space, with its diameter denoted as l_i . For 2D space, a grid field is a circular-plate area activating the grid cell. Clearly, to cover the whole space without omissions, more than one grid cell with different phases are required. The larger the ratio of λ_i to l_i , the more grid cells are needed. If there must be at least d cells responding to a spatial location, the total number of grid cells across all layers can be expressed as N :

$$N = \sum_{i=1}^m d \left(\frac{\lambda_i}{l_i} \right)^p \quad (9)$$

Apart from that, the condition $l_i \leq \lambda_{i-1}$ must be satisfied. If not, the grid cell system cannot ascertain current location when cells from both layer i and $i+1$ fire simultaneously, because the larger firing field contains more than one smaller fields, as shown in Figure 2. The condition derives $l_i \leq \lambda_i/r$. If the grid cell system must represent the space at a given constant spatial resolution R , that is, we predefined the measurement relationship between the largest scale and the smallest firing field unit:

$$R = \left(\frac{\lambda_m}{l_1} \right)^p = \left(\prod_{i=0}^{m-1} \frac{\lambda_{i+1}}{\lambda_i} \right)^p = (r^p)^m \quad (10)$$

Here we set the $\lambda_0 = l_1$. When we denote $r^p = \rho$ we get:

$$N = d \sum_{i=1}^m \left(\frac{\lambda_i}{l_i} \right)^p \geq d m r^p = d \rho \log_\rho R \quad (11)$$

By differentiation, we find that when $\rho = e$, which means $r = \sqrt[p]{e}$, we achieve the minimal number of grid cells, adhering to the principle of economy. In summary, a hierarchical grid cell representation can, with a limited population number, efficiently cover the space. The theoretically optimal scale ratio for p -dimensional space is $r = \sqrt[p]{e}$.

In the original Transformer architecture, the adjacent scale of positional encoding is described by Equation 12. For instance, when the encoding dimension d_{model} is 128, the difference in adjacent scales is $10000^{\frac{2}{128}} \approx 1.457$, whereas for an encoding dimension of 512, the difference in adjacent scales is $10000^{\frac{2}{512}} \approx 1.036$. This relationship can be expressed as follows:

$$\rho_{\text{ratio}} = \frac{10000^{\frac{2(i+1)}{d_{\text{model}}}}}{10000^{\frac{2i}{d_{\text{model}}}}} = 10000^{\frac{2}{d_{\text{model}}}} \quad (12)$$

As discussed, to avoid ambiguity in positional encoding, the maximum scale ratio for encoding in an n -dimensional space is $r = \sqrt[p]{e}$. Consequently, the minimum encoding dimension can be determined when the base is 10000. To achieve an adjacent scale difference of $\sqrt[p]{e}$, we can establish the following inequality:

$$10000^{\frac{2}{d_{\text{model}}}} \leq \sqrt[p]{e} \quad (13)$$

Taking the logarithm of both sides and solving for d_{model} :

$$\frac{2}{d_{\text{model}}} \log(10000) \leq \frac{1}{p} \log(e) \quad (14)$$

$$d_{\text{model}} \geq \frac{2 \log(10000)p}{\log(e)} \quad (15)$$

This allows us to calculate the minimum encoding dimension d_{model} that satisfies the specified adjacent scale difference.

Proposal of Grid-cell Positional Encoding (GridPE)

After demonstrating the capability of representing relative movement in space through inner product calculations and determining the optimal ratio of encoding periods, we introduce a unified positional encoding scheme for attention-based architectures. Inspired by neuroscientific principles of grid cells, our method extends the foundational ideas presented by (Su et al. 2024). While Su’s model combines absolute and relative positional encodings within a fixed framework, our schema advances this by incorporating grid cell-inspired encodings that inherently support extrapolation to higher dimensions and maintain translational invariance. Notably, in one-dimensional space, where GridPE can be expressed using a single Fourier basis, our encoding scheme is equivalent to rotational positional encoding. This demonstrates the flexibility of our approach and its alignment with established encoding strategies, further enhancing its applicability across various architectural contexts. According to Su’s model, to accommodate both absolute and relative positional encoding, the inner product of the query q and key k , which represents their similarity, can be modified as follows:

$$\langle q', k' \rangle = q^T W_m^T W_n k \quad (16)$$

Here m and n refer to the position of the query and key respectively. The multiplication of W_m and W_n is the function of the relative position $m - n$. We can encode the position m based on the grid cell encoding rationale. Assume there are d dimensions for the embedded queries and keys, we also set d layers of different scale of grid cell. Then we can set the positional code as below:

$$W_m = \begin{bmatrix} \sum_i c_i e^{j\omega_{i,1}^T m} \\ \sum_i c_i e^{j\omega_{i,2}^T m} \\ \vdots \\ \sum_i c_i e^{j\omega_{i,d}^T m} \end{bmatrix} \quad (17)$$

Here we substitute the symbol of the wave vector k with ω in case of confusion of key. We can see the inner product of the two positional codes $W_m^T W_n$ preserve the translational invariance. To fulfill the positional encoding in the neural network, we proposed several strategies as the variants to integrate the position information into the queries or keys.

Representing Encodings as Rotation Matrices If the information to be encoded (query or key) is a d -dimensional vector, and d is even, then the positional codes can be calculated as follows:

$$R_m = \begin{bmatrix} A_1 & \mathbf{0} & \cdots & \mathbf{0} \\ \mathbf{0} & A_2 & \cdots & \mathbf{0} \\ \vdots & \vdots & \ddots & \vdots \\ \mathbf{0} & \mathbf{0} & \cdots & A_{d/2} \end{bmatrix} \quad (18)$$

$$A_k = \begin{bmatrix} \Re(e^{j\omega_{k,1}^T m}) & -\Im(e^{j\omega_{k,1}^T m}) \\ \Im(e^{j\omega_{k,1}^T m}) & \Re(e^{j\omega_{k,1}^T m}) \end{bmatrix} \quad (19)$$

$$\langle \mathbf{q}', \mathbf{k}' \rangle = \mathbf{q}^T \mathbf{R}_m^T \mathbf{R}_n \mathbf{k} \quad (20)$$

The $\Re(\cdot)$ and $\Im(\cdot)$ respectively means the extraction of the real and imagery part. The purpose of this strategy is to encode the position by constructing the rotation matrix. The rotation angles comes from the grid cell Fourier functions.

Incorporating Real and Imaginary Parts into Information Vectors We can also extract the real and imagery part and add them into the information vectors, similar to the original Transformer architecture:

$$\mathbf{q}' = \Re(\mathbf{W}_m) + \Im(\mathbf{W}_m) + \mathbf{q} \quad (21)$$

After the encoding, the similarity of encoded queries and key can be calculated as vector dot product.

Preserving the Complex Form We can directly use the real part of the inner product between two sets of "complex" position encoding as the encoding product.

$$\langle \mathbf{q}', \mathbf{k}' \rangle = \mathbf{q}^T \Re(\mathbf{W}_m^H \mathbf{W}_n) \mathbf{k} \quad (22)$$

The Hermite operator means the conjugate transpose of the complex matrix.

Feature Mapping of Positional Encoding Using Deep Learning Finally, we can transform the original positional encoding by applying a trained deep neural network.

$$\langle \mathbf{q}', \mathbf{k}' \rangle = \mathbf{q}^T f_\theta(\mathbf{W}_m^T) f_\theta(\mathbf{W}_n) \mathbf{k} \quad (23)$$

where $f_\theta(\cdot)$ is a neural network projection (e.g. a multi-layer perceptrons) parameterized by θ . The projection does not change the dimension of the encoding.

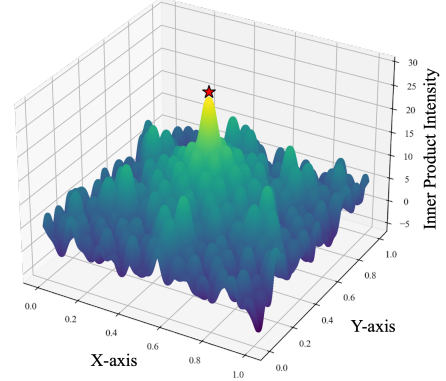
Experiments

Property of Distance Decay

We first display that our positional encoding approach exhibits the property of distance decay in any high-dimensional space. This implies that the association between two positions diminishes as the distance between them increases. We select a square area in two-dimensional space, calculating the positional encoding vector within the area as shown in Equation 17, and compute the inner products between the central "core" point and uniformly sampled points. Given that we have proven the translational invariance of the inner product, our findings remain valid when any other point is chosen as the core. Figure 3 presents the inner product surface plot and a profile plot with x fixed at 0.5.

We observe that the inner product exhibits an overall decreasing trend as the spatial distance increases, with points near the core having relatively larger inner products. Despite this, local sinusoidal fluctuations, resulting from the Fourier function form, are still evident. These calculations corroborate the effectiveness of our encoding method in representing spatial distance relationships.

Inner Product with Core Point across the Grid in 3D



Inner Product Intensity along Y-axis with Fixed X=0.0

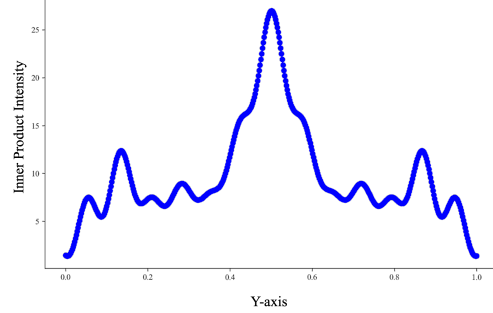


Figure 3: The inner products intensity with the core points (0.5, 0.5) of points in the unit square area. Left: the distribution of inner products is shown as a surface plot across the area. Right: a profile plot showing the inner products between core points and points with fixed $x = 0.5$.

Performance of GridPE on Visual Task

To empirically validate the capability of GridPE strategies in encoding positional information, we draw on previous research (Chu et al. 2021, 2023) and design an image classification task to evaluate neural network architectures with different positional encodings. We select the Pyramid Vision Transformer (PVT) (Wang et al. 2021) and Vision Transformer (ViT) (Dosovitskiy et al. 2020) as the base architectures.

Baseline model descriptions. PVT introduces a pyramid structure into the transformer architecture, which reduces input resolution and computational cost while enhancing performance in dense prediction tasks by effectively capturing multi-scale features. ViT, on the other hand, revolutionizes image classification by applying the transformer model to fixed-size image patches, leveraging global self-attention to model relationships across the entire image.

Dataset. We utilize the ImageNet-100 dataset, a subset of the widely recognized ImageNet dataset, to design our classification task. With its diverse and complex imagery, ImageNet-100 serves as an ideal benchmark for evaluating

the effectiveness of GridPE in encoding positional information, rigorously testing the model’s ability to handle high-dimensional and varied visual inputs. For our task, we partition 20% of the images into a validation set, while the remaining 80% are used for training, ensuring robust model evaluation and effective training during the experiment.

Implementation details. We train the neural networks on a system with an NVIDIA RTX 4090 GPU using the PyTorch framework. Models are trained for 200 epochs with the AdamW optimizer and a batch size of 32. The ‘ReduceLROnPlateau’ scheduler is employed to halve the learning rate if validation accuracy does not improve for 10 consecutive epochs, helping to fine-tune the model and prevent overfitting. PVT models use an image size of 384, while ViT models use 224. These settings ensure robust training and evaluation on the ImageNet-100 dataset.

Results and Analysis We assess the effectiveness of GridPE by comparing models with different positional encoding strategies applied to two core attention-based architectures: PVT and ViT. For PVT, we evaluate the original version without explicit two-dimensional positional encoding (PVT-o), a variant using classical sinusoidal encoding (PVT-abs) (Vaswani et al. 2017), and a model incorporating conditional positional encoding (CPVT) (Chu et al. 2023). Additionally, we introduce four GridPE-enhanced versions—GridPVT-rotate, GridPVT-complex, GridPVT-deep, and GridPVT-merge—each reflecting different grid cell-inspired positional encoding strategies. We also apply these GridPE variants to the ViT architecture to examine their impact on a simpler and less parameter-intensive model. By comparing these GridPE-enhanced versions with the baseline ViT model, we aim to elucidate the influence of GridPE across models with varying architectural complexities.

Model Name	Acc@1 (%)	Acc@5 (%)	Loss
PVT-o	84.1	96.2	1.467
CPVT	87.1	95.8	1.498
PVT-abs	85.3	96.6	1.483
GridPVT-rotate	82.3	95.7	1.511
GridPVT-complex	83.0	95.9	1.507
GridPVT-deep	84.6	97.4	1.445
GridPVT-merge	82.9	95.8	1.514
ViT	76.1	93.0	0.8234
GridViT-rotate	77.6	91.5	0.9832
GridViT-complex	78.8	93.7	0.8691
GridViT-deep	81.5	94.2	0.4676
GridViT-merge	79.0	94.0	1.083

Table 1: Comparative Analysis of Different Position Encoding Methods in Image Classification Tasks

Table 1 presents the comparative results, showing how different positional encoding strategies impact the performance of PVT and ViT models. Among these PVT models, CPVT achieves the highest top-1 accuracy (87.1%), while

GridPVT-deep excels with the best top-5 accuracy (97.4%) and the lowest loss (1.445). The convergence curves in Figure 4a reveal that PVT models generally maintain stable and efficient convergence regardless of the positional encoding used, likely due to their complex architecture and larger parameter count. This complexity allows the PVT models to capture intricate spatial relationships, minimizing the impact of different positional encodings on their convergence speed and overall performance.

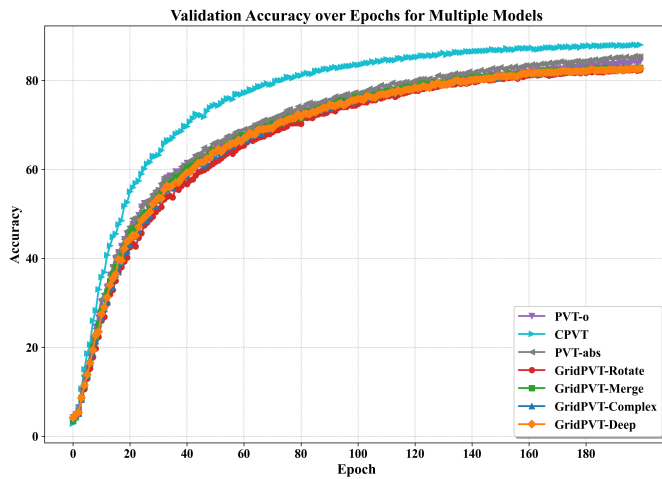
For the ViT architecture, the application of GridPE variants results in noticeable improvements in performance, as seen in Table 1. GridViT-deep emerges as the most successful variant, achieving the highest top-1 accuracy (81.5%) and the lowest loss (0.4676), representing significant gains over the baseline ViT model. The validation accuracy curves in Figure 4b highlight that ViT models, which are simpler and have fewer parameters compared to PVT models, are more sensitive to changes in positional encoding. While other variants such as GridViT-complex and GridViT-merge also outperform the baseline ViT model, they exhibit higher losses, suggesting that while GridPE can enhance accuracy, it may require further tuning to optimize efficiency and convergence. This underscores the importance of carefully matching positional encoding strategies with the model architecture to achieve the best performance outcomes.

Conclusion

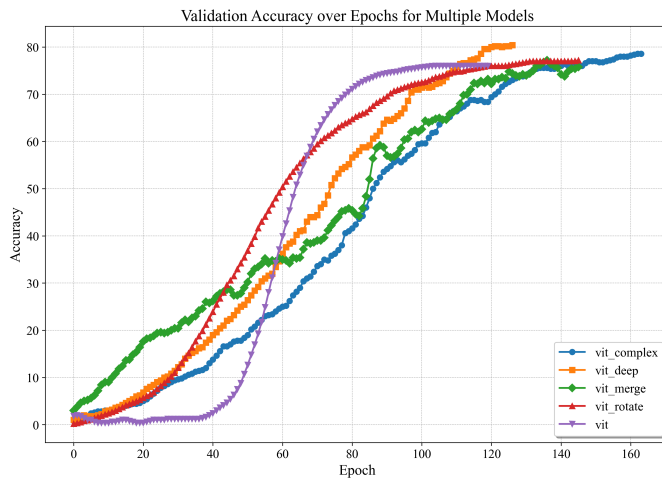
Positional encoding is essential for structuring information in neural networks, with its generality suggesting a unified algorithmic strategy that applies across visual, auditory, and linguistic domains. This study introduces GridPE, a unified framework inspired by grid cells in the mammalian brain, to enhance transformer architectures for high-dimensional data processing. GridPE captures both absolute and relative positioning, crucial for tasks involving spatial relationships. Experiments in image classification demonstrate that GridPE achieves competitive accuracy compared to state-of-the-art approaches. Its versatility and scalability across different data domains suggest promising applications in natural language processing, robotics, and spatial cognition, blending neuroscience principles with artificial intelligence.

References

- Anselmi, F.; Murray, M. M.; and Franceschiello, B. 2020. A computational model for grid maps in neural populations. *Journal of computational neuroscience*, 48(2): 149–159.
- Banino, A.; Barry, C.; Uria, B.; Blundell, C.; Lillicrap, T.; Mirowski, P.; Pritzel, A.; Chadwick, M. J.; Degris, T.; Mo-dayil, J.; et al. 2018. Vector-based navigation using grid-like representations in artificial agents. *Nature*, 557(7705): 429–433.
- Blair, H. T.; Welday, A. C.; and Zhang, K. 2007. Scale-invariant memory representations emerge from moire interference between grid fields that produce theta oscillations: a computational model. *Journal of Neuroscience*, 27(12): 3211–3229.
- Bochner, S. 2005. *Harmonic analysis and the theory of probability*. Courier Corporation.



(a) Validation Accuracy over Epochs for Multiple Variants of PVT Models.



(b) Validation Accuracy over Epochs for Multiple ViT Models.

Figure 4: Comparison of Validation Accuracy over Epochs for ViT and PVT Models.

Burak, Y.; and Fiete, I. R. 2009. Accurate path integration in continuous attractor network models of grid cells. *PLoS computational biology*, 5(2): e1000291.

Burgess, N.; Barry, C.; and O’keefe, J. 2007. An oscillatory interference model of grid cell firing. *Hippocampus*, 17(9): 801–812.

Chu, X.; Tian, Z.; Wang, Y.; Zhang, B.; Ren, H.; Wei, X.; Xia, H.; and Shen, C. 2021. Twins: Revisiting the Design of Spatial Attention in Vision Transformers. In *NeurIPS 2021*.
Chu, X.; Tian, Z.; Zhang, B.; Wang, X.; and Shen, C. 2023. Conditional Positional Encodings for Vision Transformers. In *ICLR 2023*.

Dang, S.; Wu, Y.; Yan, R.; and Tang, H. 2021. Why grid cells function as a metric for space. *Neural Networks*, 142: 128–137.

Deng, J.; Dong, W.; Socher, R.; Li, L.-J.; Li, K.; and Fei-Fei, L. 2009. Imagenet: A large-scale hierarchical image

database. In *2009 IEEE conference on computer vision and pattern recognition*, 248–255. Ieee.

Dosovitskiy, A.; Beyer, L.; Kolesnikov, A.; Weissenborn, D.; Zhai, X.; Unterthiner, T.; Dehghani, M.; Minderer, M.; Heigold, G.; Gelly, S.; et al. 2020. An image is worth 16x16 words: Transformers for image recognition at scale. *arXiv preprint arXiv:2010.11929*.

Eliav, T.; Geva-Sagiv, M.; Yartsev, M. M.; Finkelstein, A.; Rubin, A.; Las, L.; and Ulanovsky, N. 2018. Nonoscillatory phase coding and synchronization in the bat hippocampal formation. *Cell*, 175(4): 1119–1130.

Gorchetchnikov, A.; and Grossberg, S. 2007. Space, time and learning in the hippocampus: how fine spatial and temporal scales are expanded into population codes for behavioral control. *Neural Networks*, 20(2): 182–193.

Hafting, T.; Fyhn, M.; Molden, S.; Moser, M.-B.; and Moser, E. I. 2005. Microstructure of a spatial map in the entorhinal cortex. *Nature*, 436(7052): 801–806.

Hasselmo, M. E. 2008. Grid cell mechanisms and function: contributions of entorhinal persistent spiking and phase resetting. *Hippocampus*, 18(12): 1213–1229.

Krupic, J.; Burgess, N.; and O’Keefe, J. 2012. Neural representations of location composed of spatially periodic bands. *Science*, 337(6096): 853–857.

Mai, G.; Janowicz, K.; Yan, B.; Zhu, R.; Cai, L.; and Lao, N. 2020. Multi-scale representation learning for spatial feature distributions using grid cells. *arXiv preprint arXiv:2003.00824*.

Mai, G.; Xuan, Y.; Zuo, W.; He, Y.; Song, J.; Ermon, S.; Janowicz, K.; and Lao, N. 2023. Sphere2Vec: A general-purpose location representation learning over a spherical surface for large-scale geospatial predictions. *ISPRS Journal of Photogrammetry and Remote Sensing*, 202: 439–462.

Moser, E. I.; Kropff, E.; and Moser, M.-B. 2008. Place cells, grid cells, and the brain’s spatial representation system. *Annu. Rev. Neurosci.*, 31: 69–89.

O’keefe, J.; and Nadel, L. 1978. *The hippocampus as a cognitive map*. Oxford university press.

Rahimi, A.; and Recht, B. 2007. Random features for large-scale kernel machines. *Advances in neural information processing systems*, 20.

Solstad, T.; Moser, E. I.; and Einevoll, G. T. 2006. From grid cells to place cells: a mathematical model. *Hippocampus*, 16(12): 1026–1031.

Stensola, H.; Stensola, T.; Solstad, T.; Frøland, K.; Moser, M.-B.; and Moser, E. I. 2012. The entorhinal grid map is discretized. *Nature*, 492(7427): 72–78.

Su, J.; Ahmed, M.; Lu, Y.; Pan, S.; Bo, W.; and Liu, Y. 2024. Roformer: Enhanced transformer with rotary position embedding. *Neurocomputing*, 568: 127063.

Tolman, E. C. 1948. Cognitive maps in rats and men. *Psychological Review*, 55(4): 189–208. Place: US Publisher: American Psychological Association.

Vaswani, A.; Shazeer, N.; Parmar, N.; Uszkoreit, J.; Jones, L.; Gomez, A. N.; Kaiser, Ł.; and Polosukhin, I. 2017. Attention is all you need. *Advances in neural information processing systems*, 30.

- Wang, W.; Xie, E.; Li, X.; Fan, D.-P.; Song, K.; Liang, D.; Lu, T.; Luo, P.; and Shao, L. 2021. Pyramid vision transformer: A versatile backbone for dense prediction without convolutions. In *Proceedings of the IEEE/CVF international conference on computer vision*, 568–578.
- Wei, X.-X.; Prentice, J.; and Balasubramanian, V. 2015. A principle of economy predicts the functional architecture of grid cells. *Elife*, 4: e08362.
- Whittington, J. C.; McCaffary, D.; Bakermans, J. J.; and Behrens, T. E. 2022. How to build a cognitive map. *Nature neuroscience*, 25(10): 1257–1272.
- Yartsev, M. M.; Witter, M. P.; and Ulanovsky, N. 2011. Grid cells without theta oscillations in the entorhinal cortex of bats. *Nature*, 479(7371): 103–107.
- Yu, C.; Behrens, T. E.; and Burgess, N. 2020. Prediction and generalisation over directed actions by grid cells. *arXiv preprint arXiv:2006.03355*.
- Yuan, M.; Tian, B.; Shim, V. A.; Tang, H.; and Li, H. 2015. An entorhinal-hippocampal model for simultaneous cognitive map building. In *Proceedings of the AAAI Conference on Artificial Intelligence*, volume 29.